Collective-Motion-Enhanced Acceleration Sensing via an Optically Levitated Microsphere Array

Yao Li[1], Chuang Li[2,*], Jiandong Zhang[3], Ying Dong[2,†] and Huizhu Hu[1,2,4]

[1]*State Key Laboratory of Modern Optical Instrumentation, College of Optical Science and Engineering, Zhejiang University, Hangzhou 310027, China*

[2]*Research Center for Quantum Sensing, Zhejiang Lab, Hangzhou 311121, China*

[3]*School of Mathematics and Physics, Jiangsu University of Technology, Changzhou 213001, China*

[4]*State Key Laboratory, College of Optical Science and Engineering, Institute for Quantum Sensing, Zhejiang University, Hangzhou 310027, China*

Optically levitated microspheres are an excellent candidate for force and acceleration sensing. Here, we propose an acceleration-sensing protocol based on an optically levitated microsphere array (MSA). The system consists of an N-microsphere array levitated in a driven optical cavity via holographic optical tweezers. By positioning the microspheres suitably relative to the cavity, the center-of-mass (COM) mode of the collective motion of the MSA is coupled to the cavity mode. The optomechanical interaction encodes the information of acceleration that acts on the MSA onto the intracavity photons, which can then be detected directly at the output of the cavity. The optically levitated MSA distributes its mass into multiple optical traps, which not only circumvents the problem of levitating a large-mass microsphere but also leads to a significant improvement in sensitivity. Compared with the traditional single-microsphere measurement scheme, our method presents an improvement in sensitivity by a factor of $\sqrt{N}$.

I. INTRODUCTION

Optomechanics is a fascinating field that explores the interaction between optical and mechanical degrees of freedom and it has a wide range of applications in various scientific domains [1]. One of the most promising applications of optomechanics is in precision measurement, where optomechanical sensors enable the ultrasensitive detection of forces and accelerations [2–7].

Levitated optomechanics [8], where nano- and micro-objects are levitated in vacuum by optical tweezers [9–11], has emerged as a particularly promising area of research that has gained significant attention [12–20]. Optically levitated sensors provide high isolation from thermal-environment noise sources in high vacuum, enabling exceptional displacement, force, and acceleration sensitivity [21–24]. Experimental results have demonstrated a force sensitivity as low as 10^{-20} N/$\sqrt{\text{Hz}}$ [25,26] and an acceleration sensitivity below sub-μg/$\sqrt{\text{Hz}}$ (g = 9.8 m/s^2) [27–29]. Levitated optomechanical systems offer precise control of the translational and rotational degrees of freedom of the nanoparticle [30–36], making them an ideal platform for fundamental scientific research [37–47] such

as the detection of high-frequency gravitational waves [48,49], the search for dark matter [50], and the exploration of macroscopic quantum superposition with mesoscopic particles [18,51–54]. Additionally, electrostatic and magnetic levitation [8,55], as well as coupling to solid-state spin systems [56,57], have extended the capabilities of levitated optomechanics and open up new opportunities for both scientific research and technological applications.

Recently, there has been a lot of interest in the levitation and control of multiple nanoparticles using holographic optical tweezers. This is because optically trapped particle arrays have emerged as a platform for the study of complex nonequilibrium phenomena [58,59]. Holographic optical tweezers (HOTs) are a powerful technology that combines holography and optical tweezers [17,60]. The basic working principle of HOTs is to use a computer-designed diffractive optical element, such as spatial light modulators (SLMs), to split a single collimated laser beam into several separate beams, each of which is focused into an optical tweezer by a strong converging lens [61]. One of the key advantages of HOTs is the ability to manipulate multiple particles independently and precisely, allowing the creation of optically levitated nanoparticle arrays with complex structures [62].

In the fields of precision measurements and searching for new physics, detecting forces and accelerations with

*lic@zhejianglab.com
†yingdong@zhejianglab.edu.cn

increasing sensitivity is crucial [8,47]. When it comes to acceleration sensing, a large-mass nanoparticle is advantageous, as the acceleration sensitivity $\sqrt{S_a}$ is inversely proportional to its mass m [63], i.e.,

$$\sqrt{S_a} = \sqrt{\frac{2k_B T \gamma}{m}}, \qquad (1)$$

where γ is the damping rate, k_B is the Boltzmann constant, and T is the temperature of the surrounding environment. However, optically levitating a large-mass nanoparticle experimentally is a huge challenge, because laser heating constrains the maximum size of particles that can be levitated [27]. Another approach to improve sensitivity is by reducing the pressure in the surrounding environment. Levitated optomechanical experiments have been conducted at a pressure level of around 10^{-9} mbar [53, 54]. However, a further reduction in pressure is still a formidable challenge.

Here, we present an acceleration-sensing method based on an optically levitated MSA. By utilizing holographic optical tweezers, an array of nanoparticles is levitated in a Fabry-Perot cavity that is driven by an external laser beam. The nanoparticles collectively interact with the cavity mode, thus resulting in an effective coupling between a normal mode [center-of-mass (COM) mode] of the collective motion of the nanoparticles and the cavity mode. Consequently, the acceleration of the MSA can be measured by analyzing the transmission of the cavity mode. Compared to the traditional single-oscillator scheme, our protocol circumvents the problem of optically levitating a large-size (-mass) particle because the mass of the MSA is distributed into multiple optical traps. Moreover, the mass is increased with an increase in the number of trapped particles, which will lead to a significant improvement in the sensitivity of acceleration sensing.

II. SCHEME OF ACCELERATION SENSING

A. Physical model

A simplified schematic of the experimental setup is shown in Fig. 1. By employing the HOTs, an MSA containing N dielectric microspheres of mass m_i is trapped and levitated in a Fabry-Perot cavity, which is driven by an external laser beam. The position of each sphere can be independently altered by adjusting the HOTs. The transmission of the cavity mode is monitored via homodyne detection.

In this paper, we assume all the microspheres are positioned in the cavity axis and we focus on the one-dimensional motion along the cavity-axis direction. The Hamiltonian of the whole system in a frame rotating at
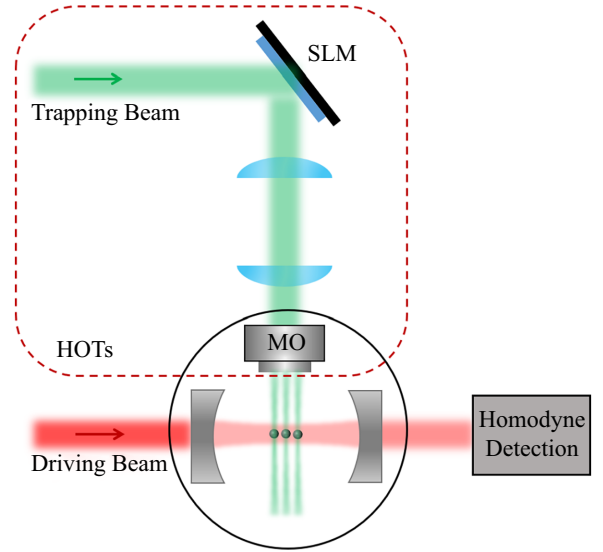

FIG. 1. A simplified schematic of the experimental setup. An MSA is levitated in a Fabry-Perot cavity by the HOTs. The cavity is driven by an external laser beam and excites a standing-wave cavity mode. The position of each sphere can be independently altered by adjusting the HOTs. The transmission of the cavity mode is monitored via homodyne detection.

pumping frequency ν_p reads

$$
\begin{aligned}
H = {}& \hbar\Delta_c \hat{a}^\dagger \hat{a} + \hbar\epsilon \left(\hat{a} + \hat{a}^\dagger\right) \\
& + \sum_{i=1}^{N} \left[\frac{\hbar\Omega_i}{2} \left(\hat{p}_i^2 + \hat{q}_i^2\right) + \hbar f_i \hat{q}_i + \hat{H}_i^{\text{Int}} \right], \qquad (2)
\end{aligned}
$$

where $\hat{a}$ is the annihilation operator of the cavity mode, $\Delta_c = \omega_c - \nu_p$ is the detuning of the cavity mode with frequency ω_c from the pumping laser, and ϵ is the pump strength. $\hat{q}_i$ and $\hat{p}_i$ denote, respectively, the dimensionless position and momentum operators of the mechanical oscillators and the Ω_i are the frequencies of the mechanical oscillators. f_i is the external force acting on each mechanical oscillator, which induces the inertial acceleration a_i via

$$f_i = \sqrt{\frac{m_i}{\hbar\Omega_i}} a_i. \qquad (3)$$

$\hat{H}_i^{\text{Int}}$ accounts for the linear coupling between the cavity mode and the mechanical oscillators. In the case that the radii of the spheres are much smaller than the cavity-mode wavelength $r_i \ll \lambda_c$, the dipole force potential created by the cavity mode can be approximated as [64]

$$\hat{U}_i^{\text{dipole}} = -\hbar U_i^0 \hat{a}^\dagger \hat{a} \cos\left[2k(q_i^{\text{eq}} + \hat{q}_i')\right], \qquad (4)$$

where $k = 2\pi/\lambda_c$ denotes the wave number of the cavity field, q_i^{eq} is the relative equilibrium position of

the ith oscillator in the cavity standing wave, $\hat{q}'_i = \sqrt{2}q^i_{zpf}\hat{q}_i$ is the position operator of the ith oscillator with zero-point fluctuation $q^i_{zpf} = \sqrt{\hbar/2m_i\Omega_i}$, and $U^0_i = (3V_i/4V_c)[(\epsilon_0 - 1)/(\epsilon_0 + 2)]\omega_c$ is a frequency shift, in which V_i and V_c are the volumes of the microspheres and the cavity, respectively, and ϵ_0 is the electric permittivity. Assuming that the oscillation of the sphere around its equilibrium position is small, one can expand the dipole force potential to first order and obtain a linear-coupling interaction Hamiltonian,

$$\hat{H}^{\mathrm{Int}}_i = \hbar g_i \hat{a}^\dagger \hat{a} \hat{q}_i, \tag{5}$$

where $g_i = 2\sqrt{2}U^0_i k q^i_{zpf} \sin[2kq^{\mathrm{eq}}_i]$ is the linear-coupling strength, the value of which can be adjusted by shifting the equilibrium positions q^{eq}_i.

B. Dynamical equations and solutions

Under the strong driving conditions, we can rewrite each operator as the sum of its classical steady-state mean value and a small quantum fluctuation operator, i.e., $\hat{a} \rightarrow \alpha + \hat{a}$, $\hat{q}_i \rightarrow q^s_i + \hat{q}_i$ and $\hat{p}_i \rightarrow p^s_i + \hat{p}_i$. Employing the standard linearization procedure [65], we obtain the quantum Langevin equations (QLEs) in terms of the quantum fluctuating operators:

$$\begin{aligned}
\dot{\hat{a}} &= -\left(i\Delta + \frac{\kappa}{2}\right)\hat{a} - \sum_i^N iG_i\hat{q}_i + \sqrt{\kappa}\hat{a}^{\mathrm{in}}, \\
\dot{\hat{q}}_i &= \Omega_i\hat{p}_i, \\
\dot{\hat{p}}_i &= -\Omega_i\hat{q}_i - \gamma_i\hat{p}_i - G_i\left(\hat{a} + \hat{a}^\dagger\right) - f_i + \hat{\xi}_i,
\end{aligned} \tag{6}$$

where we have phenomenologically introduced κ and γ_i to account for the dissipation of the cavity field and the mechanical oscillators, respectively. At the same time, we also obtain a set of classical Langevin equations (CLEs), from which the steady-state values can be figured out (for details, see the Appendix A). $\Delta = \Delta_c + \sum_i g_i q^s_i$ and $G_i = \alpha g_i$ are the effective detuning and the coupling strength, which depend on the steady-state values. The operator $\hat{a}^{\mathrm{in}}$ in Eqs. (6) accounts for the input noise of the cavity field, which has zero mean value, and the correlation function

$$\langle \hat{a}^{\mathrm{in}}(t)\hat{a}^{\mathrm{in},\dagger}(t')\rangle = \delta(t - t'), \tag{7}$$

where we have assumed that the equilibrium mean photon number of the thermal bath is

$$\bar{n}^c = \frac{1}{\exp[\hbar\omega_c/k_BT] - 1} \simeq 0$$

due to the high optical frequency $\hbar\omega_c/k_BT \gg 1$. $\hat{\xi}_i$ is the input noise of the Brownian force acting on the ith mechanical oscillator, the correlation function of which is given

by

$$\langle \hat{\xi}_i(t)\hat{\xi}_j(t')\rangle = \frac{\gamma_i}{\Omega_i}\int \frac{d\omega}{2\pi}e^{-i\omega(t-t')}\omega\left[\coth\left(\frac{\hbar\omega}{2k_BT}\right) + 1\right]\delta_{ij}, \tag{8}$$

where δ_{ij} is the Kroneker symbol. The mechanical frequencies involved are never larger than hundreds of megahertz and therefore one can make the approximation $(\gamma_i/\Omega_i)\omega\coth(\hbar\omega/2k_BT) \simeq \gamma_i(2k_BT/\hbar\Omega_i) \simeq \gamma_i(2\bar{n}^m_i + 1)$, where $\bar{n}^m_i = (\exp[\hbar\Omega_i/k_BT] - 1)^{-1}$ is the mean thermal phonon number. As a result, the correlation function of Brownian noise can be safely considered to be Markovian: [65,66], i.e.,

$$\langle \hat{\xi}_i(t)\hat{\xi}_j(t')\rangle \simeq \gamma_i(2\bar{n}^m_i + 1)\delta(t - t')\delta_{ij}. \tag{9}$$

Equations (6) show that the particles interact collectively with the cavity mode. Consequently, a normal mode of the collective motion of the MSA is coupled to the cavity mode. Here, the normal mode of collective motion refers to the synchronized movement of a system consisting of multiple particles, which couples the complex motion of individual interacting particles into simple collective motions in which the particles move in sync with the same frequency and phase [67,68]. The form of the normal mode, $\hat{Q}_{\mathrm{Norm}} = \sum_i^N G_i\hat{q}_i$, is dependent on the coupling strength between the particle and cavity mode G_i. Considering that one can choose the microspheres with an (almost) identical size, that the environments around these closely positioned microspheres (approximately in the micrometer range) are the same, and that the mechanical resonance frequency can be precisely controlled by tuning the trapping laser power, we can reasonably assume that $m_i = m$, $\gamma_i = \gamma$, and $\Omega_i = \Omega$. When all the coupling strengths are equal, i.e., $G_i = G$, a special normal mode—that is, the COM mode $\hat{Q} = \sum_i^N \hat{q}_i$—is coupled to the cavity mode. The QLEs are thus can be rewritten in closed form as follows:

$$\begin{aligned}
\dot{\hat{X}} &= \Delta\hat{Y} - \frac{\kappa}{2}\hat{X} + \sqrt{\kappa}\hat{X}^{\mathrm{in}}, \\
\dot{\hat{Y}} &= -\Delta\hat{X} - \frac{\kappa}{2}\hat{Y} - \sqrt{2}G\hat{Q} + \sqrt{\kappa}\hat{Y}^{\mathrm{in}}, \\
\ddot{\hat{Q}} &+ \gamma\dot{\hat{Q}} + \Omega^2\hat{Q} = -\sqrt{2}N\Omega G\hat{X} - \Omega F + \Omega\hat{\xi},
\end{aligned} \tag{10}$$

where $\hat{\xi} = \sum_i^N \hat{\xi}_i$ and $F = \sum_i^N f_i$ are the total Brownian-noise operator and the total external force, respectively. $\hat{X} = (\hat{a} + \hat{a}^\dagger)/\sqrt{2}$ and $\hat{Y} = (\hat{a} - \hat{a}^\dagger)/i\sqrt{2}$ are, respectively, the amplitude- and phase-quadrature operators of the cavity field. Without loss of generality, we assume that each mechanical oscillator undergoes the same acceleration, i.e., $a_i = a$, and thus the total external force can be

simplified as

$$F = Nf = N\sqrt{\frac{m}{\hbar\Omega}}a. \tag{11}$$

The QLEs given in Eqs. (10) clearly show that the information of acceleration is encoded into the cavity field mediated through the COM mode $\hat{Q}$. Since the coupling strength depends on the equilibrium of the ith microsphere, i.e., $G_i \propto \sin[2kq_i^{\text{eq}}]$, the identical coupling strength $G_i = G$ can be achieved by adjusting the equilibrium position of the microsphere using the HOTs. By setting $2kq_{i+1}^{\text{eq}} - 2kq_i^{\text{eq}} = 2n\pi$ with a positive integer $n = 1, 2, 3, \ldots$, we obtain the condition leading to the equal coupling strength as

$$\Delta q^{\text{eq}} = q_{i+1}^{\text{eq}} - q_i^{\text{eq}} = \frac{n\lambda_c}{2}, \tag{12}$$

where Δq^{eq} denotes the separation between the adjacent particles.

By Fourier transforming the QLEs in Eqs. (10) into the frequency domain and using the standard input-output relations $\hat{X}^{\text{out}} = \hat{X}^{\text{in}} - \sqrt{\kappa}\hat{X}$, one can solve the equations and obtain the power spectral density (PSD) of the output optical field in amplitude quadrature, e.g., in terms of the PSDs of acceleration and the input noise, as follows:

$$
\begin{aligned}
S_{XX}^{\text{out}}(\omega) &= \frac{N^2 m}{\hbar\Omega} |\sqrt{\kappa}H_{XF}(\omega)|^2 S_{aa}(\omega) \\
&+ |\sqrt{\kappa}H_{X\xi}(\omega)|^2 S_{\xi\xi}(\omega) \\
&+ |\sqrt{\kappa}H_{XY}(\omega)|^2 S_{YY}^{\text{in}}(\omega) \\
&+ |1 - \sqrt{\kappa}H_{XX}(\omega)|^2 S_{XX}^{\text{in}}(\omega), \tag{13}
\end{aligned}
$$

from which one can eventually solve the PSD of the acceleration in terms of the PSDs of the output optical field in amplitude quadrature and input noises, as

$$
\begin{aligned}
S_{aa}(\omega) &= \frac{\hbar\Omega}{N^2 m}\left\{ \frac{S_{XX}^{\text{out}}(\omega)}{|\sqrt{\kappa}H_{XF}(\omega)|^2} - \left|\frac{H_{X\xi}(\omega)}{H_{XF}(\omega)}\right|^2 S_{\xi\xi}(\omega) \right. \\
&- \left|\frac{H_{XY}(\omega)}{H_{XF}(\omega)}\right|^2 S_{YY}^{\text{in}}(\omega) \\
&- \left. \left|\frac{1 - \sqrt{\kappa}H_{XX}(\omega)}{\sqrt{\kappa}H_{XF}(\omega)}\right|^2 S_{XX}^{\text{in}}(\omega) \right\}, \tag{14}
\end{aligned}
$$

where the symbol $H_{AB}(\omega)$ denotes the response function (the concrete form can be found in the Appendix A) from the external noise or signal source B to the detectable quadrature A and the PSD for quantity $\hat{O}$ is defined as $S_{OO}(\omega) = \int_{-\infty}^{\infty}\langle\hat{O}^\dagger(t)\hat{O}(0)\rangle \exp[i\omega t]dt$. It is noteworthy that the area under the experimentally measured PSD

yields the variance of the acceleration [1], i.e.,

$$\langle a^2 \rangle = \int_{-\infty}^{\infty} S_{aa}(\omega)\frac{d\omega}{2\pi}. \tag{15}$$

Thus one can acquire both the frequency and amplitude information of the acceleration from its PSD. The Brownian noise can be calculated from Eq. (9) as $S_{\xi_i\xi_i}(\omega) = \gamma_i(2\bar{n}_i^m + 1)$ and the optical input noisy PSDs are simply $S_{XX}^{\text{in}}(\omega) = S_{YY}^{\text{in}}(\omega) = 1/2$ for the vacuum optical reservoir. After measuring the PSD $S_{XX}^{\text{out}}(\omega)$ in amplitude quadrature (or $S_{YY}^{\text{out}}(\omega)$ in phase quadrature), which can be done directly with homodyne or heterodyne detection [18,35, 53], we will eventually be able to carry out the PSD of the acceleration.

III. IMPROVEMENT OF ACCELERATION SENSITIVITY THROUGH COLLECTIVE MOTION

To estimate the acceleration $S_{aa}(\omega)$, we invert the measured PSD of the output optical field in Eq. (13) and obtain

$$\frac{\hbar\Omega}{N^2 m}\frac{S_{XX}^{\text{out}}(\omega)}{|\sqrt{\kappa}H_{XF}(\omega)|^2} = S_{aa}(\omega) + \frac{\hbar\Omega}{N^2 m}\left[S_{\xi\xi}(\omega) + S_{\text{opt}}^{\text{in}}(\omega)\right], \tag{16}$$

where the optical input noise is

$$S_{\text{opt}}^{\text{in}}(\omega) = \left|\frac{H_{XY}(\omega)}{H_{XF}(\omega)}\right|^2 S_{YY}^{\text{in}}(\omega) + \left|\frac{1 - \sqrt{\kappa}H_{XX}(\omega)}{\sqrt{\kappa}H_{XF}(\omega)}\right|^2 S_{XX}^{\text{in}}(\omega). \tag{17}$$

Therefore, the signal-to-noise ratio (SNR) turns out to be

$$S_{\text{SNR}}(\omega) = \sqrt{\frac{S_{aa}(\omega)}{\frac{\hbar\Omega}{N^2 m}\left[S_{\xi\xi}(\omega) + S_{\text{opt}}^{\text{in}}(\omega)\right]}}. \tag{18}$$

By setting $S_{\text{SNR}}(\omega) = 1$ as the condition that defines sensitivity, we obtain the acceleration sensitivity as

$$\sqrt{S_a^{(N)}(\omega)} = \sqrt{\frac{\hbar\Omega}{N^2 m}\left[S_{\xi\xi}(\omega) + S_{\text{opt}}^{\text{in}}(\omega)\right]}. \tag{19}$$

The Brownian noise acting on each mechanical oscillator is independent and uncorrelated; thus the PSD of the total Brownian noise $S_{\xi\xi}(\omega)$ is the sum of the PSD of the Brownian noise acting on every single mechanical oscillator $S_{\xi_i\xi_i}(\omega)$, which is given by

$$S_{\xi\xi}(\omega) = \sum_i^N S_{\xi_i\xi_i}(\omega) = N S_{\xi\xi}^{(1)}(\omega), \tag{20}$$

where $S_{\xi\xi}^{(1)}(\omega) = \gamma(2\bar{n}^m + 1)$ is the PSD of the Brownian noise acting on a single mechanical oscillator. Therefore,

the acceleration sensitivity is simplified as

$$\sqrt{S_a^{(N)}(\omega)} = \sqrt{\frac{\hbar\Omega}{m} \left[\frac{S_{\xi\xi}^{(1)}(\omega)}{N} + \frac{S_{\text{opt}}^{\text{in}}(\omega)}{N^2} \right]}. \qquad (21)$$

This equation clearly shows that the acceleration sensitivity improves with an increase in the number of oscillators N. In the limit of $k_B T \gg \hbar\Omega$, i.e., the dissipative dynamics of the system are dominated solely by the thermal noise, the optical input noise can be omitted. As a result, we find an improvement in sensitivity by a factor of $\sqrt{N}$ compared with the standard single-oscillator acceleration-sensing scheme [see Eq. (1)]:

$$\sqrt{S_a^{(N)}} \approx \sqrt{\frac{\hbar\Omega}{Nm}\gamma\left(2\bar{n}^m + 1\right)} \approx \sqrt{\frac{S_a}{N}}. \qquad (22)$$

The analytical derivations indicate that this scheme can improve the sensitivity by a factor of $\sqrt{N}$ not only in acceleration sensing but also in force sensing. Thus our scheme also applies to the detection of the forces that depend on mass, such as non-Newtonian forces [47].

Figure 2(a) shows the acceleration sensitivity as a function of the frequency for different numbers of oscillators N. The results indicate that the acceleration sensitivity improves with an increase in the oscillator number N. The acceleration sensitivity drops at the mechanical resonance frequency Ω due to the Lorentzian-like line-shape response function. Figure 2(b) shows the acceleration sensitivity at the mechanical resonance frequency (normalized with the sensitivity for $N = 1$) as a function of the number of oscillators N. The sensitivity represents a significant improvement in increasing the oscillator number.

IV. NUMERICAL SIMULATION

We numerically simulate the dynamics of the whole optomechanical system via the following Markovian master equation:

$$\dot{\rho} = \frac{1}{i\hbar}\left[\hat{\rho}, \hat{H}_L\right] + \mathcal{L}\left(\hat{\rho}\right), \qquad (23)$$

where $\hat{\rho}$ is the density operator of the optomechanical system, $\hat{H}_L = \hbar\Delta_c\hat{a}^\dagger\hat{a} + \sum_{i=1}^{N}(\hbar\Omega/2)\left(\hat{p}_i^2 + \hat{q}_i^2\right) + \hbar f_i(t)\hat{q}_i + \hbar G\left(\hat{a}^\dagger + \hat{a}\right)\hat{q}_i$ is the linearized Hamiltonian, and $f_i(t)$ is the time-dependent external force acting on each mechanical oscillator, which induces an acceleration via the relation in Eq. (3), i.e., one can obtain the acceleration through $a_i(t) = \sqrt{\hbar\Omega_i/m_i}f_i(t)$. The Lindblad superoperator describing the
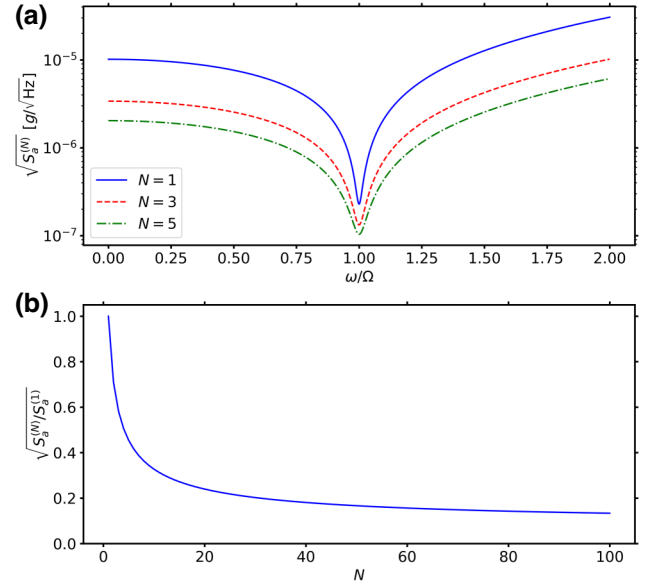

FIG. 2. (a) The acceleration sensitivity as a function of the frequency for different numbers of oscillators. (b) The acceleration sensitivity at the mechanical resonance frequency (normalized with the sensitivity for $N = 1$) as a function of the number of oscillators N. The parameters are set as $\Omega/2\pi = 100$ kHz, $\Delta/2\pi = 500$ kHz, $G/2\pi = 10$ kHz [69,70], $\kappa/2\pi = 1$ GHz, $T = 300$ K, $\gamma/2\pi = 100$ μHz [71], and $r = 5$ μm.

system dissipation reads

$$\mathcal{L}\left(\hat{\rho}\right) = \frac{\kappa}{2}\left(2\hat{a}\hat{\rho}\hat{a}^\dagger - \hat{a}^\dagger\hat{a}\hat{\rho} - \hat{\rho}\hat{a}^\dagger\hat{a}\right) + \sum_{i=1}^{N}\frac{\gamma}{2}\left(\bar{n}_i^m + 1\right)$$
$$\times\left(2\hat{b}_i\hat{\rho}\hat{b}_i^\dagger - \hat{b}_i^\dagger\hat{b}_i\hat{\rho} - \hat{\rho}\hat{b}_i^\dagger\hat{b}_i\right)$$
$$+ \frac{\gamma}{2}\bar{n}_i^m\left(2\hat{b}_i^\dagger\hat{\rho}\hat{b}_i - \hat{b}_i\hat{b}_i^\dagger\hat{\rho} - \hat{\rho}\hat{b}_i\hat{b}_i^\dagger\right), \qquad (24)$$

where $\hat{b}_i$ is the mechanical annihilation operator of the ith sphere. In the simulation, we assume that the external forces acting on each oscillator are identical and in the form of $f(t) = A_f\cos\Omega_f t$, with the amplitude A_f and the frequency Ω_f. We simulate the dynamical evolution of a three-microsphere array and plot the PSDs of the output optical field in amplitude quadrature, $\hat{X}^{\text{out}}$, and the total force, $F = \sum_{i=1}^{3}f_i(t)$ (insets), for different frequencies Ω_f in Fig. 3. Two peaks at the frequencies corresponding to that of the external force are observed, which confirms that the optomechanical interaction encodes the information of the collective motion induced by the external acceleration into the cavity field. We also note that the height of the peaks corresponding to the external force in the optical PSD increases along with the frequency of the acceleration approaching the mechanical resonance frequency due to the Lorentzian-like line-shape response functions. In the insets, the two PSDs of the forces corresponding to
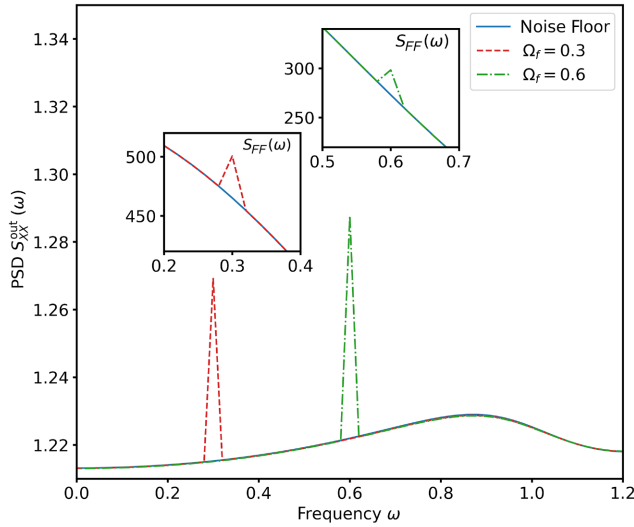
FIG. 3. The PSDs of the output optical field in amplitude quadrature $\hat{X}^{\text{out}}$ for different external forces, which are obtained from the numerical simulation for a three-microsphere array. The insets show the corresponding PSDs of the forces. The parameters are set as follows: the mechanical frequency $\Omega_{1,2,3} = 1$, the damping rate $\gamma = 0.5$, the thermal phonon number $\bar{n}_{1,2,3}^m = 0.1$, the cavity detuning $\Delta = 5$, the cavity decay rate $\kappa = 10$, the coupling strength $G = 0.1$, and the external force $f_{1,2,3}(t) = 0.1\cos(0.3t)$ and $f_{1,2,3}(t) = 0.1\cos(0.6t)$, respectively.

the frequencies $\Omega_f = 0.3$ and $\Omega_f = 0.6$ have an almost equal height (filled area) because of the same amplitude $A_f = 0.1$. According to the connection between the amplitude and the PSD in Eq. (15), we integrate the PSD around the peak $\Omega_f = 0.3$ ($\Omega_f = 0.6$) over the noise floor in the insets and obtain the variance $\langle F^2 \rangle|_{\Omega_f=0.3} \approx 0.059$ ($\langle F^2 \rangle|_{\Omega_f=0.6} \approx 0.040$). This result is consistent with the variance obtained from the analytical expression: $F(t) = 3f(t) = 0.3\cos(\Omega_f t)$ with $\langle F^2 \rangle = 0.045$.

V. FEASIBILITY ANALYSIS OF THE PROTOCOL

Our theoretical scheme is based on a multi-oscillator-cavity optomechanical system that can be realized experimentally by employing holographic optical tweezers levitating many nanoparticles in a driven optical cavity. Following Ref. [58], a feasible experimental realization is shown as follows.

As shown in Fig. 1, the trapping beam is expanded to overfill the apertures of the spatial light modulator (SLM) and the microscope objective (MO). The laser beams created by the SLM are imaged with a $4f$ image system onto the MO, creating an array of tightly focused optical tweezers that trap the particle array in a Fabry-Perot cavity. The cavity is driven by another external laser beam (driven beam), allowing the excited intracavity field (cavity mode)

to interact with the MSA. The transmission of the intracavity field is monitored through homodyne detection. The coherent scattering and interference effects between the trapping and driven beams are suppressed both by orienting the tweezer polarization along the cavity axis to minimize the mode overlap and by tuning the two lasers far apart in frequency space.

By manipulating the phase (and amplitude) of the laser beam using the spatial light modulator, we can precisely trap and move particles, ensuring that the separation between the adjacent particles satisfies the condition in Eq. (12) such that the collective COM mode of the MSA is coupled to the cavity mode. In experiments, the separation between two adjacent optical traps created by holographic optical tweezers is several microns due to the waist of the traps and the size of the trapped particle, requiring a selection of large integer n. Since the loading of the particle array is probabilistic, a rearrangement protocol utilizing an auxiliary beam [59] can be implemented to improve the success probability of loading. In a real experiment, the phase noise (or, equivalently, the frequency noise) will impact the performance of acceleration sensing. We can use a filtering cavity to suppress it [35,70]. In addition, a method of far-field wave-front shaping [72,73] may be employed to cool the motion of particles.

VI. SUMMARY AND OUTLOOK

In conclusion, we have proposed a protocol for acceleration sensing by using an optically levitated MSA. With the help of holographic optical tweezers, an MSA containing N microspheres is levitated in a driven Fabry-Perot cavity. By suitably adjusting the positions of the microspheres in the cavity, the optomechanical interaction encodes the acceleration information acting on the MSA onto the intracavity photons that can be measured at the cavity output via homodyne detection.

Since the mass of the MSA is distributed among multiple optical traps, our protocol can overcome the difficulty of optically levitating a single large-mass microsphere. Although magnetic trapping has the capability to levitate larger-size (or -mass) particles, it has some drawbacks in sensing, such as low trapping frequencies ($\leq$ 1 kHz), control of static trap potentials, and low compatibility with optical measurements [8]. Moreover, the collective motion of the MSA enhances acceleration sensitivity by increasing the number of levitated microspheres. Compared to the traditional acceleration scheme where a single microsphere of mass m is levitated, our scheme can achieve an improvement by a factor of $\sqrt{N}$ in sensitivity when employing an MSA containing N m-mass microspheres.

In the future, along with the development of a holographic optical-tweezers technique [61] in high vacuum and optical measurement methods, our protocol may be

extended to a large three-dimensional sensing array that will possibly enable full-profile imaging and dynamical-evolution monitoring of a force field in real time. In addition, the optically levitated MSA itself provides a platform to investigate quantum entanglement and quantum correlation [58,74].

APPENDIX A: DERIVATION OF THE PSD OF ACCELERATION

Here, we present the detailed derivation of the PSD of the acceleration in Eq. (14). Starting from the Hamiltonian given in Eq. (2), by employing the standard linearization procedure [65], we obtain the quantum Langevin equations QLEs given in Eqs. (6) in terms of the quantum fluctuation operators, together with a set of classical Langevin equations (CLEs) in terms of the classical mean values,

$$
\begin{aligned}
\dot{\alpha} &= -\left(i\Delta + \frac{\kappa}{2}\right)\alpha - i\epsilon, \\
\dot{q}_i^s &= \Omega_i p_i^s, \\
\dot{p}_i^s &= -\Omega_i q_i^s - \gamma_i p_i^s - g_i|\alpha|^2.
\end{aligned}
\tag{A1}
$$

By setting the time derivatives to zero in Eqs. (A1), one obtains the steady-state mean values as

$$
\begin{aligned}
\alpha &= \frac{-i\epsilon}{i\Delta + \kappa/2}, \\
p_i^s &= 0, \\
q_i^s &= -\frac{g_i|\alpha|^2}{\Omega_i},
\end{aligned}
\tag{A2}
$$

which are used to determine the effective detuning and the coupling strength in QLEs [see Eqs. (6)].

To solve the QLEs in Eqs. (10), we transform them into the frequency domain via the Fourier transformation $\hat{\tilde{O}}(\omega) = \int_{-\infty}^{\infty} \hat{O}(t)\exp[i\omega t]dt$, where the operators with and without a tilde denote the same quantity in the time and the frequency domain, respectively. The QLEs in the

frequency domain are given by

$$
\begin{aligned}
\left(\frac{\kappa}{2} - i\omega\right)\hat{\tilde{X}}(\omega) &= \sqrt{\kappa}\hat{\tilde{X}}^{\text{in}}(\omega) + \Delta\hat{\tilde{Y}}(\omega), \\
\left(\frac{\kappa}{2} - i\omega\right)\hat{\tilde{Y}}(\omega) &= \sqrt{\kappa}\hat{\tilde{Y}}^{\text{in}}(\omega) - \Delta\hat{\tilde{X}}(\omega) - \sqrt{2}G\hat{\tilde{Q}}(\omega), \\
\chi_m^{-1}(\omega)\hat{\tilde{Q}}(\omega) &= \hat{\tilde{\xi}}(\omega) - \sqrt{2}NG\hat{\tilde{X}}(\omega) - \tilde{F}(\omega),
\end{aligned}
\tag{A3}
$$

where $\chi_m(\omega) = \Omega/(\Omega^2 - \omega^2 - i\gamma\omega)$ is the bare mechanical response function (susceptibility). By solving Eqs. (A3), we obtain the amplitude- and phase-quadrature operators of the cavity field as

$$
\hat{\tilde{X}}(\omega) = H_{XF}(\omega)\tilde{F}(\omega) + H_{X\xi}(\omega)\hat{\tilde{\xi}}(\omega) + H_{XY}(\omega)\hat{\tilde{Y}}^{\text{in}}(\omega) \\
+ H_{XX}(\omega)\hat{\tilde{X}}^{\text{in}}(\omega),
\tag{A4a}
$$

$$
\hat{\tilde{Y}}(\omega) = H_{YF}(\omega)\tilde{F}(\omega) + H_{Y\xi}(\omega)\hat{\tilde{\xi}}(\omega) + H_{YX}(\omega)\hat{\tilde{X}}^{\text{in}}(\omega) \\
+ H_{YY}(\omega)\hat{\tilde{Y}}^{\text{in}}(\omega),
\tag{A4b}
$$

with the corresponding response functions

$$
H_{XF}(\omega) = -H_{X\xi}(\omega) = -\sqrt{2}G\chi_m(\omega)\chi(\omega), \tag{A5a}
$$

$$
H_{XY}(\omega) = -\sqrt{\kappa}\chi(\omega), \tag{A5b}
$$

$$
H_{XX}(\omega) = -\frac{\frac{\kappa}{2} - i\omega}{\Delta}\sqrt{\kappa}\chi(\omega), \tag{A5c}
$$

$$
H_{YF}(\omega) = -\frac{\sqrt{2}G\chi_m(\omega)\left(\frac{\kappa}{2} - i\omega\right)}{2}\chi(\omega), \tag{A5d}
$$

$$
H_{Y\xi}(\omega) = -H_{YF}(\omega), \tag{A5e}
$$

$$
H_{YX}(\omega) = -\frac{\sqrt{\kappa}\left(\frac{\kappa}{2} - i\omega\right)^2}{2\Delta}\chi(\omega) - \frac{\sqrt{\kappa}}{\Delta}, \tag{A5f}
$$

$$
H_{YY}(\omega) = -\frac{\sqrt{\kappa}\left(\frac{\kappa}{2} - i\omega\right)}{2}\chi(\omega), \tag{A5g}
$$

where

$$
\chi(\omega) = \frac{1}{2NG^2\chi_m(\omega) - \Delta - \frac{(\frac{\kappa}{2} - i\omega)^2}{\Delta}}. \tag{A6}
$$

With the solutions of $\hat{\tilde{X}}(\omega)$ and $\hat{\tilde{Y}}(\omega)$, the PSDs of the cavity-field quadrature operators are given by

$$
S_{XX}(\omega) = |H_{XF}(\omega)|^2 S_{FF}(\omega) + |H_{X\xi}(\omega)|^2 S_{\xi\xi}(\omega) \\
+ |H_{XY}(\omega)|^2 S_{YY}^{\text{in}}(\omega) + |H_{XX}(\omega)|^2 S_{XX}^{\text{in}}(\omega),
\tag{A7a}
$$

$$
S_{YY}(\omega) = |H_{YF}(\omega)|^2 S_{FF}(\omega) + |H_{Y\xi}(\omega)|^2 S_{\xi\xi}(\omega) \\
+ |H_{YX}(\omega)|^2 S_{XX}^{\text{in}}(\omega) + |H_{YY}(\omega)|^2 S_{YY}^{\text{in}}(\omega),
\tag{A7b}
$$

$$S_{FF}(\omega) = \frac{S_{XX}(\omega)}{|H_{XF}(\omega)|^2} - \frac{|H_{X\xi}(\omega)|^2}{|H_{XF}(\omega)|^2} S_{\xi\xi}(\omega) - \frac{|H_{XY}(\omega)|^2}{|H_{XF}(\omega)|^2} S_{YY}^{\text{in}}(\omega) - \frac{|H_{XX}(\omega)|^2}{|H_{XF}(\omega)|^2} S_{XX}^{\text{in}}(\omega)$$

$$= \frac{S_{YY}(\omega)}{|H_{YF}(\omega)|^2} - \frac{|H_{Y\xi}(\omega)|^2}{|H_{YF}(\omega)|^2} S_{\xi\xi}(\omega) - \frac{|H_{YX}(\omega)|^2}{|H_{YF}(\omega)|^2} S_{XX}^{\text{in}}(\omega) - \frac{|H_{YY}(\omega)|^2}{|H_{YF}(\omega)|^2} S_{YY}^{\text{in}}(\omega). \tag{A8}$$

The PSDs of the input noise can be calculated via the correlation functions in Eqs. (7) and (9) and the exact results are given by

$$S_{XX}^{\text{in}}(\omega) = S_{YY}^{\text{in}}(\omega) = \frac{1}{2},$$
$$S_{\xi_i \xi_i}(\omega) = \gamma_i \left(2\bar{n}_i^m + 1\right). \tag{A9}$$

To establish the connection between $S_{FF}(\omega)$ and the quantities that are measurable directly in experiments, we need to further consult quantum input-output theory. By substituting the input-output relations $\hat{X}^{\text{out}} = \hat{X}^{\text{in}} - \sqrt{\kappa}\hat{X}$ and $\hat{Y}^{\text{out}} = \hat{Y}^{\text{in}} - \sqrt{\kappa}\hat{Y}$ into Eqs. (A4), we obtain the amplitude- and phase-quadrature operators of the output optical field as

$$\hat{\tilde{X}}^{\text{out}}(\omega) = -\sqrt{\kappa}\left[H_{XF}(\omega)\tilde{F}(\omega) + H_{X\xi}(\omega)\hat{\tilde{\xi}}(\omega)\right.$$
$$\left. + H_{XY}(\omega)\hat{\tilde{Y}}^{\text{in}}(\omega)\right]$$
$$+ \left[1 - \sqrt{\kappa}H_{XX}(\omega)\right]\hat{\tilde{X}}^{\text{in}}(\omega), \tag{A10}$$

$$\hat{\tilde{Y}}^{\text{out}}(\omega) = -\sqrt{\kappa}\left[H_{YF}(\omega)\tilde{F}(\omega) + H_{Y\xi}(\omega)\hat{\tilde{\xi}}(\omega)\right.$$
$$\left. + H_{YX}(\omega)\hat{\tilde{X}}^{\text{in}}(\omega)\right]$$
$$+ \left[1 - \sqrt{\kappa}H_{YY}(\omega)\right]\hat{\tilde{Y}}^{\text{in}}(\omega). \tag{A11}$$

By using the relation between the force and acceleration in Eq. (3), one can obtain the PSD of the output optical field in amplitude and phase as

$$S_{XX}^{\text{out}}(\omega) = \frac{N^2 m}{\hbar\Omega}|\sqrt{\kappa}H_{XF}(\omega)|^2 S_{aa}(\omega) + |\sqrt{\kappa}H_{X\xi}(\omega)|^2 S_{\xi\xi}(\omega)$$
$$+ |\sqrt{\kappa}H_{XY}(\omega)|^2 S_{YY}^{\text{in}}(\omega)$$
$$+ |1 - \sqrt{\kappa}H_{XX}(\omega)|^2 S_{XX}^{\text{in}}(\omega), \tag{A12a}$$

$$S_{YY}^{\text{out}}(\omega) = \frac{N^2 m}{\hbar\Omega}|\sqrt{\kappa}H_{YF}(\omega)|^2 S_{aa}(\omega) + |\sqrt{\kappa}H_{Y\xi}(\omega)|^2 S_{\xi\xi}(\omega)$$
$$+ |\sqrt{\kappa}H_{YX}(\omega)|^2 S_{XX}^{\text{in}}(\omega)$$
$$+ |1 - \sqrt{\kappa}H_{YY}(\omega)|^2 S_{YY}^{\text{in}}(\omega). \tag{A12b}$$

By solving the above equations, we obtain the eventual expression for the PSD of the acceleration determined by the output optical field and the input noises as follows:

$$S_{aa}(\omega) = \frac{\hbar\Omega}{N^2 m}\left\{\frac{S_{XX}^{\text{out}}(\omega)}{|\sqrt{\kappa}H_{XF}(\omega)|^2} - \left|\frac{H_{X\xi}(\omega)}{H_{XF}(\omega)}\right|^2 S_{\xi\xi}(\omega)\right.$$
$$- \left|\frac{H_{XY}(\omega)}{H_{XF}(\omega)}\right|^2 S_{YY}^{\text{in}}(\omega)$$
$$\left. - \left|\frac{1 - \sqrt{\kappa}H_{XX}(\omega)}{\sqrt{\kappa}H_{XF}(\omega)}\right|^2 S_{XX}^{\text{in}}(\omega)\right\}$$
$$= \frac{\hbar\Omega}{N^2 m}\left\{\frac{S_{YY}^{\text{out}}(\omega)}{|\sqrt{\kappa}H_{YF}(\omega)|^2} - \left|\frac{H_{Y\xi}(\omega)}{H_{YF}(\omega)}\right|^2 S_{\xi\xi}(\omega)\right.$$
$$- \left|\frac{H_{YX}(\omega)}{H_{YF}(\omega)}\right|^2 S_{XX}^{\text{in}}(\omega)$$
$$\left. - \left|\frac{1 - \sqrt{\kappa}H_{YY}(\omega)}{\sqrt{\kappa}H_{YF}(\omega)}\right|^2 S_{YY}^{\text{in}}(\omega)\right\}. \tag{A13}$$

In the experiments, the output-optical-field PSD $S_{XX}^{\text{out}}(\omega)$ in the amplitude-quadrature operator or $S_{YY}^{\text{out}}(\omega)$ in the phase-quadrature operator can be obtained directly by optical homodyne and heterodyne detection.

[1] M. Aspelmeyer, T. J. Kippenberg, and F. Marquardt, Cavity optomechanics, Rev. Mod. Phys. **86**, 1391 (2014).

[2] G. Anetsberger, O. Arcizet, Q. P. Unterreithmeier, R. Rivière, A. Schliesser, E. M. Weig, J. P. Kotthaus, and T. J. Kippenberg, Near-field cavity optomechanics with nanomechanical oscillators, Nat. Phys. **5**, 909 (2009).

[3] E. Gavartin, P. Verlot, and T. J. Kippenberg, A hybrid on-chip optomechanical transducer for ultrasensitive force measurements, Nat. Nanotechnol. **7**, 509 (2012).

[4] A. G. Krause, M. Winger, T. D. Blasius, Q. Lin, and O. Painter, A high-resolution microchip optomechanical accelerometer, Nat. Photonics **6**, 768 (2012).

[5] F. Guzmán Cervantes, L. Kumanchik, J. Pratt, and J. M. Taylor, High sensitivity optomechanical reference accelerometer over 10 kHz, Appl. Phys. Lett. **104**, 221111 (2014).

[6] D. Mason, J. Chen, M. Rossi, Y. Tsaturyan, and A. Schliesser, Continuous force and displacement measurement below the standard quantum limit, Nat. Phys. **15**, 745 (2019).

[7] W. Zhao, S.-D. Zhang, A. Miranowicz, and H. Jing, Weak-force sensing with squeezed optomechanics, Sci. China Phys. Mech. Astron. **63**, 224211 (2020).

[8] C. Gonzalez-Ballestero, M. Aspelmeyer, L. Novotny, R. Quidant, and O. Romero-Isart, Levitodynamics: Levitation and control of microscopic objects in vacuum, Science **374**, eabg3027 (2021).

[9] A. Ashkin and J. Dziedzic, Optical levitation by radiation pressure, Appl. Phys. Lett. **19**, 283 (1971).

[10] A. Ashkin and J. Dziedzic, Optical levitation in high vacuum, Appl. Phys. Lett. **28**, 333 (1976).

[11] A. Ashkin and J. Dziedzic, Feedback stabilization of optically levitated particles, Appl. Phys. Lett. **30**, 202 (1977).

[12] A. Ashkin, J. M. Dziedzic, and T. Yamane, Optical trapping and manipulation of single cells using infrared laser beams, Nature **330**, 769 (1987).

[13] A. Ashkin and J. M. Dziedzic, Optical trapping and manipulation of viruses and bacteria, Science **235**, 1517 (1987).

[14] F. M. Fazal and S. M. Block, Optical tweezers study life under tension, Nat. Photonics **5**, 318 (2011).

[15] K. Dholakia and T. Čižmár, Shaping the future of manipulation, Nat. Photonics **5**, 335 (2011).

[16] M. Padgett and R. Bowman, Tweezers with a twist, Nat. Photonics **5**, 343 (2011).

[17] O. M. Maragò, P. H. Jones, P. G. Gucciardi, G. Volpe, and A. C. Ferrari, Optical trapping and manipulation of nanostructures, Nat. Nanotechnol. **8**, 807 (2013).

[18] U. Delić, M. Reisenbauer, K. Dare, D. Grass, V. Vuletić, N. Kiesel, and M. Aspelmeyer, Cooling of a levitated nanoparticle to the motional quantum ground state, Science **367**, 892 (2020).

[19] A. de los Ríos Sommer, N. Meyer, and R. Quidant, Strong optomechanical coupling at room temperature by coherent scattering, Nat. Commun. **12**, 276 (2021).

[20] T. Kuang, R. Huang, W. Xiong, Y. Zuo, X. Han, F. Nori, C.-W. Qiu, H. Luo, H. Jing, and G. Xiao, Nonlinear multi-frequency phonon lasers with active levitated optomechanics, Nat. Phys. **19**, 414 (2023).

[21] G. Ranjit, D. P. Atherton, J. H. Stutz, M. Cunningham, and A. A. Geraci, Attonewton force detection using microspheres in a dual-beam optical trap in high vacuum, Phys. Rev. A **91**, 051805 (2015).

[22] G. Ranjit, M. Cunningham, K. Casey, and A. A. Geraci, Zeptonewton force sensing with nanospheres in an optical lattice, Phys. Rev. A **93**, 053801 (2016).

[23] D. Hempston, J. Vovrosh, M. Toroš, G. Winstone, M. Rashid, and H. Ulbricht, Force sensing with an optically levitated charged nanoparticle, Appl. Phys. Lett. **111**, 133111 (2017).

[24] C. P. Blakemore, A. D. Rider, S. Roy, Q. Wang, A. Kawasaki, and G. Gratta, Three-dimensional force-field microscopy with optically levitated microspheres, Phys. Rev. A **99**, 023816 (2019).

[25] F. Tebbenjohanns, M. Frimmer, A. Militaru, V. Jain, and L. Novotny, Cold Damping of an Optically Levitated Nanoparticle to Microkelvin Temperatures, Phys. Rev. Lett. **122**, 223601 (2019).

[26] F. Tebbenjohanns, M. Frimmer, V. Jain, D. Windey, and L. Novotny, Motional Sideband Asymmetry of a Nanoparticle Optically Levitated in Free Space, Phys. Rev. Lett. **124**, 013603 (2020).

[27] F. Monteiro, S. Ghosh, A. G. Fine, and D. C. Moore, Optical levitation of 10-ng spheres with nano-*g* acceleration sensitivity, Phys. Rev. A **96**, 063841 (2017).

[28] A. D. Rider, C. P. Blakemore, G. Gratta, and D. C. Moore, Single-beam dielectric-microsphere trapping with optical heterodyne detection, Phys. Rev. A **97**, 013842 (2018).

[29] F. Monteiro, W. Li, G. Afek, C.-L. Li, M. Mossman, and D. C. Moore, Force and acceleration sensing with optically levitated nanogram masses at microkelvin temperatures, Phys. Rev. A **101**, 053835 (2020).

[30] P. Barker, Doppler Cooling a Microsphere, Phys. Rev. Lett. **105**, 073002 (2010).

[31] J. Gieseler, B. Deutsch, R. Quidant, and L. Novotny, Sub-kelvin Parametric Feedback Cooling of a Laser-Trapped Nanoparticle, Phys. Rev. Lett. **109**, 103603 (2012).

[32] N. Kiesel, F. Blaser, U. Delić, D. Grass, R. Kaltenbaek, and M. Aspelmeyer, Cavity cooling of an optically levitated submicron particle, Proc. Natl. Acad. Sci. **110**, 14180 (2013).

[33] J. Millen, P. Fonseca, T. Mavrogordatos, T. Monteiro, and P. Barker, Cavity Cooling a Single Charged Levitated Nanosphere, Phys. Rev. Lett. **114**, 123602 (2015).

[34] E. Hebestreit, M. Frimmer, R. Reimann, and L. Novotny, Sensing Static Forces with Free-Falling Nanoparticles, Phys. Rev. Lett. **121**, 063602 (2018).

[35] U. Delić, M. Reisenbauer, D. Grass, N. Kiesel, V. Vuletić, and M. Aspelmeyer, Cavity Cooling of a Levitated Nanosphere by Coherent Scattering, Phys. Rev. Lett. **122**, 123602 (2019).

[36] T. M. Hoang, Y. Ma, J. Ahn, J. Bang, F. Robicheaux, Z.-Q. Yin, and T. Li, Torsional Optomechanics of a Levitated Nonspherical Nanoparticle, Phys. Rev. Lett. **117**, 123604 (2016).

[37] T. Li, S. Kheifets, D. Medellin, and M. G. Raizen, Measurement of the instantaneous velocity of a Brownian particle, Science **328**, 1673 (2010).

[38] T. Li and M. G. Raizen, Brownian motion at short time scales, Ann. Phys. **525**, 281 (2013).

[39] J. Gieseler, L. Novotny, and R. Quidant, Thermal nonlinearities in a nanomechanical oscillator, Nat. Phys. **9**, 806 (2013).

[40] D. C. Moore, A. D. Rider, and G. Gratta, Search for Millicharged Particles Using Optically Levitated Microspheres, Phys. Rev. Lett. **113**, 251801 (2014).

[41] J. Gieseler, R. Quidant, C. Dellago, and L. Novotny, Dynamic relaxation of a levitated nanoparticle from a nonequilibrium steady state, Nat. Nanotechnol. **9**, 358 (2014).

[42] V. Jain, J. Gieseler, C. Moritz, C. Dellago, R. Quidant, and L. Novotny, Direct Measurement of Photon Recoil from a Levitated Nanoparticle, Phys. Rev. Lett. **116**, 243601 (2016).

[43] A. D. Rider, D. C. Moore, C. P. Blakemore, M. Louis, M. Lu, and G. Gratta, Search for Screened Interactions Associated with Dark Energy below the 100 μm Length Scale, Phys. Rev. Lett. **117**, 101101 (2016).

[44] L. Rondin, J. Gieseler, F. Ricci, R. Quidant, C. Dellago, and L. Novotny, Direct measurement of Kramers turnover

with a levitated nanoparticle, Nat. Nanotechnol. **12**, 1130 (2017).

[45] W. Nie, Y. Lan, Y. Li, and S. Zhu, Generating large steady-state optomechanical entanglement by the action of Casimir force, Sci. China Phys. Mech. Astron. **57**, 2276 (2014).

[46] D. Carney, G. Krnjaic, D. C. Moore, C. A. Regal, G. Afek, S. Bhave, B. Brubaker, T. Corbitt, J. Cripe, and N. Crisosto, *et al.*, Mechanical quantum sensing in the search for dark matter, Quantum Sci. Technol. **6**, 024002 (2021).

[47] D. C. Moore and A. A. Geraci, Searching for new physics using optically levitated sensors, Quantum Sci. Technol. **6**, 014008 (2021).

[48] A. Arvanitaki and A. A. Geraci, Detecting High-Frequency Gravitational Waves with Optically Levitated Sensors, Phys. Rev. Lett. **110**, 071105 (2013).

[49] G. Winstone, Z. Wang, S. Klomp, G. R. Felsted, A. Laeuger, C. Gupta, D. Grass, N. Aggarwal, J. Sprague, and P. J. Pauzauskie, *et al.*, Optical Trapping of High-Aspect-Ratio NaYF Hexagonal Prisms for kHz-MHz Gravitational Wave Detectors, Phys. Rev. Lett. **129**, 053604 (2022).

[50] F. Monteiro, G. Afek, D. Carney, G. Krnjaic, J. Wang, and D. C. Moore, Search for Composite Dark Matter with Optically Levitated Sensors, Phys. Rev. Lett. **125**, 181102 (2020).

[51] O. Romero-Isart, M. L. Juan, R. Quidant, and J. I. Cirac, Toward quantum superposition of living organisms, New J. Phys. **12**, 033015 (2010).

[52] O. Romero-Isart, A. C. Pflanzer, F. Blaser, R. Kaltenbaek, N. Kiesel, M. Aspelmeyer, and J. I. Cirac, Large Quantum Superpositions and Interference of Massive Nanometer-Sized Objects, Phys. Rev. Lett. **107**, 020405 (2011).

[53] L. Magrini, P. Rosenzweig, C. Bach, A. Deutschmann-Olek, S. G. Hofer, S. Hong, N. Kiesel, A. Kugi, and M. Aspelmeyer, Real-time optimal quantum control of mechanical motion at room temperature, Nature **595**, 373 (2021).

[54] F. Tebbenjohanns, M. L. Mattana, M. Rossi, M. Frimmer, and L. Novotny, Quantum control of a nanoparticle optically levitated in cryogenic free space, Nature **595**, 378 (2021).

[55] C. W. Lewandowski, T. D. Knowles, Z. B. Etienne, and B. D'Urso, High-Sensitivity Accelerometry with a Feedback-Cooled Magnetically Levitated Microsphere, Phys. Rev. Appl. **15**, 014050 (2021).

[56] T. M. Hoang, J. Ahn, J. Bang, and T. Li, Electron spin control of optically levitated nanodiamonds in vacuum, Nat. Commun. **7**, 12250 (2016).

[57] J. Gieseler, A. Kabcenell, E. Rosenfeld, J. Schaefer, A. Safira, M. J. Schuetz, C. Gonzalez-Ballestero, C. C. Rusconi, O. Romero-Isart, and M. D. Lukin, Single-Spin Magnetomechanics with Levitated Micromagnets, Phys. Rev. Lett. **124**, 163604 (2020).

[58] J. Rieser, M. A. Ciampini, H. Rudolph, N. Kiesel, K. Hornberger, B. A. Stickler, M. Aspelmeyer, and U. Delić, Tunable light-induced dipole-dipole interaction between optically levitated nanoparticles, Science **377**, 987 (2022).

[59] J. Yan, X. Yu, Z. V. Han, T. Li, and J. Zhang, On-demand assembly of optically levitated nanoparticle arrays in vacuum, Photonics Res. **11**, 600 (2023).

[60] J. E. Curtis, B. A. Koss, and D. G. Grier, Dynamic holographic optical tweezers, Opt. Commun. **207**, 169 (2002).

[61] Y. Yang, Y.-X. Ren, M. Chen, Y. Arita, and C. Rosales-Guzmán, Optical trapping with structured light: A review, Adv. Photonics **3**, 034001 (2021).

[62] J. Gieseler, J. R. Gomez-Solano, A. Magazzù, I. P. Castillo, L. P. García, M. Gironella-Torrent, X. Viader-Godoy, F. Ritort, G. Pesce, and A. V. Arzola, *et al.*, Optical tweezers—from calibration to applications: a tutorial, Adv. Opt. Photonics **13**, 74 (2021).

[63] J. Millen, T. S. Monteiro, R. Pettit, and A. N. Vamivakas, Optomechanics with levitated particles, Rep. Progr. Phys. **83**, 026401 (2020).

[64] D. E. Chang, C. Regal, S. Papp, D. Wilson, J. Ye, O. Painter, H. J. Kimble, and P. Zoller, Cavity opto-mechanics using an optically levitated nanosphere, Proc. Natl. Acad. Sci. **107**, 1005 (2010).

[65] C. Genes, D. Vitali, P. Tombesi, S. Gigan, and M. Aspelmeyer, Ground-state cooling of a micromechanical oscillator: Comparing cold damping and cavity-assisted cooling schemes, Phys. Rev. A **77**, 033804 (2008).

[66] C. Genes, D. Vitali, and P. Tombesi, Simultaneous cooling and entanglement of mechanical modes of a micromirror in an optical cavity, New J. Phys. **10**, 095009 (2008).

[67] D. Watson, Normal modes for *N* identical particles: A study of the evolution of collective behavior from few-body to many-body, Ann. Phys. (NY) **419**, 168219 (2020).

[68] D. Watson, Analytic-normal-mode frequencies for *N* identical particles: The microscopic dynamics underlying the emergence and stability of excitation gaps from BCS to unitarity, Phys. Rev. A **104**, 033320 (2021).

[69] N. Meyer, A. De los Rios Sommer, P. Mestres, J. Gieseler, V. Jain, L. Novotny, and R. Quidant, Resolved-Sideband Cooling of a Levitated Nanoparticle in the Presence of Laser Phase Noise, Phys. Rev. Lett. **123**, 153601 (2019).

[70] U. Delić, D. Grass, M. Reisenbauer, T. Damm, M. Weitz, N. Kiesel, and M. Aspelmeyer, Levitated cavity optomechanics in high vacuum, Quantum Sci. Technol. **5**, 025006 (2020).

[71] L. Martinetz, K. Hornberger, and B. A. Stickler, Gas-induced friction and diffusion of rigid rotors, Phys. Rev. E. **97**, 052112 (2018).

[72] J. Hüpfl, N. Bachelard, M. Kaczvinszki, M. Horodynski, M. Kühmayer, and S. Rotter, Optimal cooling of multiple levitated particles: Theory of far-field wavefront shaping, Phys. Rev. A **107**, 023112 (2023).

[73] J. Hüpfl, N. Bachelard, M. Kaczvinszki, M. Horodynski, M. Kühmayer, and S. Rotter, Optimal Cooling of Multiple Levitated Particles through Far-Field Wavefront Shaping, Phys. Rev. Lett. **130**, 083203 (2023).

[74] H. Rudolph, U. Delić, M. Aspelmeyer, K. Hornberger, and B. A. Stickler, Force-Gradient Sensing and Entanglement via Feedback Cooling of Interacting Nanoparticles, Phys. Rev. Lett. **129**, 193602 (2022).